

CNWRA A center of excellence in earth sciences and engineering

A Division of Southwest Research Institute™
6220 Culebra Road • San Antonio, Texas, U.S.A. 78228-5166
(210) 522-5160 • Fax (210) 522-5155

October 1, 2002
Contract No. NRC-02-02-012
Account No. 20.06002.01.061

U.S. Nuclear Regulatory Commission
ATTN: Dr. Philip S. Justus
Office of Nuclear Material Safety and Safeguards
TWFN Mail Stop 7 C6
Washington, DC 20555

Subject: Programmatic Review of Revised Journal Article

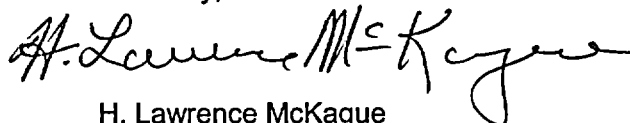
Dear Dr. Justus:

Attached is the revised Intermediate Milestone 01402.471.230, Fault displacement gradients at Yucca Mountain, Nevada—Journal Article. This manuscript has been revised to comply with each of the programmatic review comments provided in the September 19, 2002, letter from Justus to McKague. This revised manuscript is being sent to NRC for programmatic acceptance.

This deliverable describes and applies a technique to provide a qualitative assessment of distributive deformation (i.e., fracture and small scale faulting) associated with faulting. Two aspects of distributed displacement are investigated, deformation that forms parallel to a fault as a result of the displacement gradient along a fault and deformation that develops perpendicular to a fault as a result of displacement on overlapping adjacent faults. As a demonstration, this technique is applied to the displacement gradients on the Ghost Dance and Abandoned Wash faults. Increased distributed deformation occurs where the deformation gradients are high between both faults. As a result of this assessment, the paper concludes that distributed deformation is variable in the Yucca Mountain area. Therefore, if DOE expands the repository area, the characteristics of deformation in the characterized block cannot, a priori, be extrapolated into the expansion blocks without some additional examination of fractures and small faults in those new areas.

After NRC acceptance, this paper will be submitted to the Journal of Geophysical Research. If you have any questions, please contact Dr. David Ferrill at 210-522-6082 or me at 210-522-5183.

Sincerely,



H. Lawrence McKague
GLGP Element Manager

rae
Attachment

cc. J. Linehan	B. Meehan	S. Wastler	W. Patrick	N. Franklin
W. Reamer	L. Campbell	C. Trotter	B. Sagar	D. Waiting
D. DeMarco	J. Greeves	K. Stablein	CNWRA Dirs/EM (ltr only)	J. Stamatakos
D. Riffle	J. Schlueter		D. Ferrill	T. Nagy (SwRI Contracts)
			D. Sims	A. Morris

D:\GLGP Group\letters\sds\Cy-2002\paper-10-01-2002hlm.wpd



Washington Office • Twinbrook Metro Plaza #210
12300 Twinbrook Parkway • Rockville, Maryland 20852-1606

Fault displacement gradients at Yucca Mountain, Nevada

Alan P. Morris¹, David A. Ferrill², Darrell W. Sims², Nathan Franklin²,

Deborah J. Waiting²

¹Department of Earth and Environmental Science, University of Texas at San Antonio,

San Antonio, TX 78249, USA

²CNWR, Southwest Research Institute, San Antonio, TX 78238-5166, USA

For submission to the Journal of Geophysical Research

October 2002

Abstract. Yucca Mountain, Nevada, is the sole candidate site for underground disposal of high-level radioactive waste in the United States. The mountain is composed of Tertiary (12.8 Ma to 10 Ma) volcanic tuff, cut by west-dipping normal faults that divide the mountain into north-trending, east-dipping cuestas. Characterization by the U.S. Department of Energy (DOE) has focused on mapping lithostratigraphic units, faults, and fractures. Faults and fractures are important to repository design because they affect seismic hazard, rockfall, and fluid transmissivity in the surrounding rock mass. Geologic maps and detailed studies of rock pavements and tunnel walls reveal that faults and fractures within Yucca Mountain are not uniform in orientation or intensity. We investigate two aspects of distributed deformation arising from fault displacement gradients at Yucca Mountain. First, fault-parallel strains (elongation

parallel to cutoff lines where stratigraphic horizons intersect fault planes) develop as a result of fault displacement gradients. Using existing data, we analyze the likely state of strain in fault blocks at Yucca Mountain. Second, fault-strike-perpendicular strains can develop where two normal faults propagate past each other. A component of total displacement is distributed into the surrounding rock to produce synthetic layer dip or a network of smaller faults and fractures. There is a demonstrable relationship between displacement gradients on the Ghost Dance and Abandoned Wash faults and fault and fracture intensity at smaller scales. We find that small-scale faulting and fracturing at Yucca Mountain is variable and is strongly controlled by larger scale fault system architecture.

1. Introduction

Yucca Mountain, Nevada is located within the southwestern part of the Basin and Range physiographic province, on the margin of the Walker Lane (Fig. 1). It is the proposed site for the permanent disposal of high-level radioactive waste in the United States. The region is characterized by strike-slip and extensional deformation that has been active since the beginning of the Cenozoic (65 Ma) [see for example Snow and Wernicke, 2000]. The region remains tectonically active as indicated by evidence for Quaternary (including Holocene) to present-day faulting [Harmsen, 1994; Simonds et al., 1995; Ferrill et al., 1996a,b], and Quaternary volcanism [Connor and Hill, 1995; Connor et al., 2000]. Yucca Mountain itself is composed of faulted and fractured Miocene volcanic tuffs erupted from calderas in the Southwest Nevada Volcanic Field 15 to 9 million years ago [Sawyer et al., 1994]. The Tiva Canyon Tuff (12.7 Ma) of the

Paintbrush Group makes up the main surface exposures of Yucca Mountain. The proposed repository would be hosted within the Topopah Spring Tuff (12.8 Ma), also of the Paintbrush Group. Angular unconformities and fault-related depocenters within the tuff sequence indicate that faulting and tuff deposition were synchronous at Yucca Mountain [e.g., Carr, 1990; Day et al., 1998b; Fridrich, 1999]. Most faults at Yucca Mountain are either north-trending normal faults or northwest-trending, dextral strike-slip faults. The larger faults in these two orientations bound the fault blocks of Yucca Mountain (Fig. 1). Some northwest-trending faults are dominantly normal faults, accommodating extension in relay ramps between overlapping normal faults [Ferrill et al., 1999a].

The fault and fracture framework of Yucca Mountain and its environs are important to technical considerations with respect to the location, design, and long term performance of the proposed waste repository. DOE has responsibility for characterizing Yucca Mountain as a proposed high level radioactive waste repository site, and the design of the proposed repository. Faults and fractures provide potential pathways for fluid movement, and bound blocks of rocks that may fall from the walls and ceiling of excavated drifts. Therefore, the fault and fracture framework is a key factor in repository design and performance. Thus far, detailed fault and fracture characterization at Yucca Mountain has concentrated on an area between the Solitario Canyon and Bow Ridge faults (Fig. 1b), which contains the area referred to as the main repository (upper block) and the lower block [CRWMS M&O, 2001]. These two faults have maximum throws of 450 m and 150 m respectively, and are two of the largest faults that cut Yucca Mountain. Two tunnels, the Exploratory Studies Facility (ESF) and Enhanced Characterization of the Repository Block (ECRB) have been excavated in order to aid the

characterization of the main repository block with respect to rock type, faults, and fractures [Mongano et al., 1999; CRWMS M&O, 2000] (Fig. 1b). A wealth of information has been obtained to that end. However, the detailed data have not been linked to the larger structural elements of Yucca Mountain, and no models exist that will assist in the prediction of small faults and fractures in areas where no tunnels have been excavated. In this paper, we use existing data, including that acquired by DOE, to evaluate displacement patterns on mapped faults at Yucca Mountain in order to understand structural controls on small-scale faulting and fracturing at Yucca Mountain. Based on this analysis, we find that in areas where detailed studies have been conducted, displacement gradients on mapped faults can be used as indicators of distributed deformation at smaller scales within the adjacent rock.

2. Background

Surface exposures at Yucca Mountain consist of faulted and fractured Miocene silicic volcanic rocks, primarily the Tiva Canyon Tuff of the Paintbrush Group [Sawyer et al., 1994]. Also part of the Paintbrush Group, but less well-exposed than and stratigraphically below the Tiva Canyon Tuff, is the Topopah Spring Tuff. DOE has designated a series of welded units within the Topopah Spring Tuff as the proposed repository host horizon (RHH). Specifically, the RHH consists of the lower third of the upper lithophysal zone, and the middle nonlithophysal, lower lithophysal, and lower nonlithophysal zones of the crystal-poor member of the Topopah Spring Tuff [CRWMS M&O, 2001]. The top of the RHH is represented as a horizon within the

DOE Geologic Framework Model version 3.1 [CRWMS M&O, 2000], which is a three-dimensional interpretation of the structure and stratigraphy at Yucca Mountain (Fig. 2a,b).

The structural geology of Yucca Mountain is dominated by west-dipping, extensional faults with strike trends between 000° and 030° (Fig. 2). Faulting developed in the Paintbrush Group tuffs at Yucca Mountain over the last 13 million years in a stress system with a vertical σ_1 , initially with σ_3 directed EW then evolving to the current situation with σ_3 directed toward 300° [Zoback et al., 1981; Morris et al., 1996]. In addition to the dominant normal faults, small numbers of strike-slip and reverse faults have been mapped [Day et al., 1998a,b; Mongano et al., 1999]. West-dipping, normal faults define the primary fault architecture of western Yucca Mountain [Ferrill et al., 1999a]. Slip on these faults has generated the eastward-dipping fault blocks that characterize the area.

Thus far, fault characterization at Yucca Mountain has progressed along three tracks. First, the area has been mapped by traditional field geological methods at a variety of scales [Scott and Bonk, 1984; Simonds et al., 1995; Day et al., 1998a,b]. Second, fault and fracture data has been collected from detailed pavement mapping at the surface of Yucca Mountain [e.g., Barton and Hsieh, 1989; Barton and Larsen, 1995; Barton et al., 1993; Sweetkind et al., 1997] with the goal of determining the influence of these structures on the infiltration of surface water into the subsurface, and as analogs for fracturing that might be encountered in the subsurface. Third, the walls of the ESF and ECRB have provided a wealth of detailed fault and fracture data from mapping and detailed line surveys conducted during the active tunneling phase [Mongano et al., 1999; CRWMS M&O, 2000]. Traditional geological mapping is capable of detecting and representing faults with displacements greater than about 1.5 m under favorable circumstances or

greater than 5 m elsewhere [Day et al. 1998a,b], whereas mapping of tunnel walls, where colluvium and vegetation do not obscure the rock, recorded faults with displacements as small as 0.02 m [Mongano et al., 1999; CRWMS M&O, 2000].

Larger (field-mappable) faults are important indicators of the overall structure and fault block deformation at Yucca Mountain [e.g., Young et al., 1992a,b; Ferrill and Morris, 2001]. Smaller faults are more difficult to detect using surface geological mapping techniques but are more numerous than larger faults. For example, the North Ramp of the ESF traverses the mapped traces of 14 faults with displacements of 5 m to 50 m [Day et al., 1998a,b], whereas mapping of the tunnel walls (Appendix 1) of the North Ramp identified 262 faults with displacements as small as 0.02 m. Although small faults do not accommodate a major component of regional-scale deformation, they do influence permeability architecture, rockfall potential, failure strength and fracture characteristics [U.S. Department of Energy, 1998].

3. Fault displacement gradients, faults and fractures

Wherever faults exhibit displacement gradients, strain is transferred into adjacent fault blocks and the intensity of the resultant deformation is commensurate with the steepness of the displacement gradient. Two primary manifestations of this strain transfer in the case of extensional normal faults are: (i) cutoff parallel elongation [Ferrill and Morris, 2001] (Fig. 3a), and (ii) strike-perpendicular distributed deformation in zones of displacement deficit, which has been recognized in the Canyonlands (Utah) [Trudgill and Cartwright, 1994] and the English Midlands Coalfield [Peacock and Sanderson, 1994; Huggins et al., 1995; Childs et al., 1995]

(Fig. 3b). Both of these strain transfer mechanisms can be recognized in the Ghost Dance—Abandoned Wash fault system at Yucca Mountain (Fig. 2b).

3.1. Cutoff-parallel elongation

Fault-parallel elongations experienced by rock adjacent to faults are determined by fault displacement gradients, fault slip vectors, and initial stratal orientations [Ferrill and Morris, 2001]. Elongation parallel to the stratal cutoff line (line of intersection between rock strata and fault plane) can be positive (length increase) or negative (length decrease) and depends only on angular relationships [Ferrill and Morris, 2001]. Therefore, the elongation can be calculated for sections of a fault between cutoff line data points. Details of stratal cutoff lines for all principal geologic strata (horizons) at Yucca Mountain can be extracted from the DOE Geologic Framework Model [CRWMS M&O, 2000] (Fig. 2a). The resulting data can be assembled into a 3D fault gap model for any given horizon. In this paper we use a fault gap model for the top of the RHH generated from data within the DOE Geologic Framework Model [CRWMS M&O, 2000] (Fig. 2b) because it is the top of the lithologic package that DOE has selected to host the proposed repository.

3.1.1. Fault slip vectors

Fault slip vectors are required for our analysis. Using the 3D fault gap model, detailed geometry of the fault surfaces between offset cutoff lines can be generated (Fig. 2b). These surfaces can then be used to determine the slip vector field throughout the study area. This is done by using slip tendency analysis [Morris et al., 1996] to investigate a range of stress systems

likely to have been extant at the time of faulting. In computing slip tendency, the directions of maximum resolved shear stress within a fault surface are computed. For any portion of the fault surface, the direction of maximum resolved shear stress is the likely slip direction [e.g., Bott, 1959; Morris et al., 1996]. Each stress system will yield a unique slip vector field. By using a range of stress systems likely to have been operating during faulting, a range of likely slip vector fields can be computed, and their effects on cutoff elongation can be examined.

The period of most active faulting at Yucca Mountain is generally thought to have been during the Miocene (13 to 10 Ma) [Sawyer et al., 1994; Morris et al., 1996; Snow and Wernicke, 2000]. At that time, the orientation of extension (i.e., minimum principal stress) was between WSW (260°) and NW - SE (300°) [Zoback et al., 1981; Morris et al., 1996]. Vertical principal stress was determined primarily by lithostatic pressure, which is approximately 21 MPa at a depth of about 1 km for rocks with densities similar to those at Yucca Mountain [Ferrill et al., 1999b]. In order for the rocks to have been close to failure, and thus to have experienced active faulting, the differential stress ($\sigma_1 - \sigma_3$) must have been approximately 15 MPa [Hoek and Brown, 1988; Mandl, 1988], therefore the minimum stress (σ_3) would have been on the order of 6 MPa. Given these two constraints, σ_2 could have varied within these limits. High values of σ_2 [low values of R, where $R = (\sigma_1 - \sigma_2)/(\sigma_1 - \sigma_3)$] give rise to conditions conducive to both normal and strike-slip faulting [Morris et al., 1996], and to a large number of mapped fault traces at Yucca Mountain that would have experienced cutoff-parallel elongation (Appendix 2). Lower σ_2 (and higher R) values would give rise to less strike-slip faulting and a smaller number of fault traces that would have experienced cut-off parallel elongation (Appendix 2).

Data from borehole breakouts, active faulting, earthquake nodal planes, and fault orientation indicate that Yucca Mountain currently experiences a normal faulting regional stress system with σ_3 oriented approximately WNW (300° azimuth), and a σ_2 value close to that of σ_1 [Stock et al., 1985; Stock and Healy, 1988; Harmsen, 1994; Morris et al., 1996; Ferrill et al., 1999b]. This stress system accounts for the dominance of normal faulting in the area and the synchronous oblique-slip to strike-slip activity on many NW-striking faults. It is also consistent with interpretations of the slip events associated with the 1992 Little Skull Mountain earthquake [Stock and Healy, 1988; Harmsen, 1994; Morris et al., 1996] which occurred at a depth of about 8 km, 16 km ESE of Yucca Mountain.

Models of the tectonic evolution of North America during the Cenozoic in which the Juan de Fuca Ridge was subducted beneath North America creating the San Andreas fault system [Atwater, 1970] explain the transition of the Great Basin from compressional to extensional tectonics. Within this context, extension at Yucca Mountain has reached its current orientation by clockwise rotation of the stress field since about 20 Ma [Zoback et al., 1981; Morris et al., 1996]. Zoback et al. [1981] show an orientation of approximately WSW for horizontal extension during the time period 20 Ma to 10 Ma and an extension direction of WNW from 10 Ma to the present [Zoback et al., 1981]. Strikes of normal faults that cut the 12.8 Ma and younger volcanic rocks at Yucca Mountain show a pronounced maximum from 005° to 015° as seen in a length-weighted circular histogram (Fig. 4a). A heave-weighted circular histogram of normal fault strike directions (Fig. 4b) exhibits a similar, but broader maximum (from 355° to 015°). Variability in the orientations of normal faults could indicate rotation of extension direction with time, however, the great preponderance of data indicating an approximately west-

directed extension direction (azimuth of 265° to 285° ; Fig. 4a,b,c,d) suggests that most deformation occurred or at least initiated early in the rotation history. In the context of the analysis presented in this paper, stress rotation during the last 12.8 Ma modifies the detailed character and distribution of cutoff elongation, but does not increase or decrease the length of mapped fault traces (Appendix 2 F through J).

3.1.2. Initial stratal orientation

The orientation of a stratal cutoff line with respect to the slip vector influences the nature and magnitude of the elongation experienced by that cutoff line [Ferrill and Morris, 2001]. In the case of the volcanic tuffs at Yucca Mountain, strata were probably horizontal prior to faulting. However, as faulting progressed, an east dip would have developed in fault blocks. Increasing east dip of strata modifies the detailed character and distribution of cutoff elongation (illustrated by parts K through O in Appendix 2). In addition, the rotation of the regional extension direction from 265° to 300° would have progressively rotated the average stratal dip direction towards ESE.

3.2. Progressive deformation at Yucca Mountain

Deformation in fault blocks starts with the initiation of fault displacement and continues to accumulate over time with each increment of fault slip. This progressive deformation of fault blocks is in accord with changing stress state, fault geometry, and stratal orientation. The deformation state at any given time is the result of this accumulated deformation. Single maps of fault cutoff elongation of the form illustrated in each element of Appendix 2 cannot capture the

full deformation history. For example, early in the history of faulting, when the regional extension direction was approximately 265° , there would have been fewer, shorter, and smaller (in terms of displacement) faults at Yucca Mountain than are currently present. Extension direction has rotated over time, and as faults grew the slip vectors on those faults would have changed concomitantly with the changing stress conditions and fault orientations. Fault growth would also have controlled stratal dip in fault blocks and, consequently, cutoff line orientations would have evolved through time.

Many faults in Appendix 2, especially those with NW-SE strikes are modeled to have experienced significant negative cutoff elongations (shortening parallel to cutoff lines). The maps in Appendix 2 are constructed using all the present-day faults represented in the DOE Geologic Framework Model [CRWMS M&O, 2000], and, for each case, all faults are subjected to the same regional stress system and conditions of initial stratal orientation. Faults with orientations that deviate markedly from the regional average probably initiated in response to local variations in the regional stress system (the result of displacement gradients on the larger faults), and therefore the cutoff elongations modeled here would only apply when the local perturbation has been relieved by slip on that fault or faults. Once the local perturbation has been relieved and the fault responds to the full regional stress field, the modeled elongations of Appendix 2 would become relevant, and in appropriate conditions might represent the current situation on such a fault.

Complex though this evolution appears, it is possible to place reasonable bounds on some of the major determining conditions. The earliest extension direction experienced by the volcanic rocks at Yucca Mountain was probably 265° (Zoback et al., 1981). At that time, the newly

erupted rocks were probably close to horizontal in orientation. The strong preferred orientation of all faults (Fig. 4) and the common occurrence of near strike-slip motion on NW-SE trending faults indicates a stress magnitude ratio R that is low, approximately 0.25 to 0.3 [Morris et al., 1996]. Therefore, at about 13 Ma the cutoff elongation strains at Yucca Mountain could be portrayed by Fig. 5a. The principal source of uncertainty in Fig. 5a is the number of faults represented; it is likely that many of the faults shown would not have existed and those that did were shorter and accommodated less displacement than those in Fig. 5a. Currently, the regional extension direction is 300° , the stress magnitude ratio R remains low at approximately 0.25 to 0.3 [Morris et al., 1996], and the stratal dip is approximately 8° E {an average based on data from the DOE Geologic Framework Model [CRWMS M&O, 2000]}. Thus, Fig. 5b represents the cutoff elongation strain resulting from the latest increment of fault slip at Yucca Mountain. Constraints on young faulting activity are provided by the mapping of Simonds et al. [1995]. Their results show that the western Yucca Mountain fault system (especially the Windy Wash fault) has been active in the late Quaternary (Fig. 5b). Their mapping provides only a minimum estimate of Quaternary fault activity, however, because bedrock against bedrock fault slip is difficult to date [Simonds et al., 1995]. Figs. 5a and 5b, therefore, place reasonable bounds on the earliest and latest increments of cutoff elongation strain at Yucca Mountain.

3.3. Strike-perpendicular distributed deformation

Displacement patterns on the four dominant faults at Yucca Mountain (Fig. 6) indicate that they have operated as part of a segmented fault system in which the collective assemblage of faults have a coherent cumulative displacement [e.g., Peacock and Sanderson, 1994; Huggins et

al., 1995; Dawers and Anders, 1995], and therefore have the potential to rupture in concert in the event of a major earthquake [Ferrill et al., 1999a]. The Paintbrush Canyon and Solitario Canyon faults, for example, have an antipathetic displacement relationship south of 4076000 (UTM northing in meters) whereas the cumulative (combined) heave across the two faults varies smoothly (Fig.6); north of 4076000 the antipathetic relationship continues, although the cumulative heave of these faults decreases. This local decrease (deficit) in cumulative heave is in part compensated for by the presence of both the Windy Wash and Fatigue Wash faults. Further apparent heave deficit in the cumulative heave profile is not real, but rather is the result of data truncation on the Northern Windy Wash and Fatigue faults at the western edge of the DOE Geologic Framework Model [CRWMS M&O, 2000] volume. Transfer of displacement between two overlapping extensional faults can be accomplished in a number of ways, for example increased stratal dip in the area of interaction is commonly observed [Huggins et al., 1995]. Less commonly reported is an increase in the number of smaller faults and fractures contributing to the regional extension. Such an increase, however, is an important component of fault block deformation in at least one location at Yucca Mountain.

4. Ghost Dance—Abandoned Wash fault system

Using a combination of geologic maps and data from the DOE Geologic Framework Model [CRWMS M&O, 2000], we have identified an area of interaction between the Ghost Dance and Abandoned Wash faults [Area 4 in figure 9a of Ferrill and Morris, 2001]. This area is of especial interest because the Ghost Dance fault is pierced by the ESF (Fig. 7a). This area

represents one of the few opportunities to evaluate extremely detailed fault and fracture data in the context of larger faults mapped by traditional field geological methods. Mapping of the ESF Main Drift (approximately NS section) identified a 750 to 800 m long zone within the Topopah Spring Tuff in which fracture frequency averages 4.2 fractures per meter (21 fractures per 5 meter interval) [Mongano et al., 1999; CRWMS M&O, 2000]. This zone is referred to as the Intensely Fractured Zone (IFZ), and is dominated by fractures and faults that have strikes between 115° (at the north end) and 150° (at the south end) [Mongano et al., 1999; CRWMS M&O, 2000] (Fig. 7c). The Main Drift of the ESF runs parallel to, and less than 250 m west of, the Ghost Dance fault within its hanging wall. The IFZ is associated with the segment of highest displacement on the Ghost Dance fault [Mongano et al., 1999; CRWMS M&O, 2000] (Fig. 7b). Also plotted in Fig. 7c is a 5 meter running average of fracture frequencies along the ESF Main Drift wherever this running average exceeds 20 fractures per 5-meter interval. Black lines at an angle to the Main Drift indicate the dominant fracture orientation for each 500 meter segment of the Drift [Mongano et al., 1999]. Orientation of the dominant fracture trends (strikes) along the Main Drift contrast sharply with the NS strikes of the bounding faults. In fact, the NW-SE dominant fracture trend seen in the Main Drift contrasts with the dominant fault trends at Yucca Mountain in general (compare dominant fracture trends in Fig. 7c with Fig. 4a through c).

Most fractures within the IFZ are thought to be cooling joints influenced by extension shortly after eruption of the tuffs [Buesch and Spengler, 1998]. Cutoff elongation caused by slip on the Ghost Dance fault would have been appropriately oriented (sub-parallel to the strike of the fault) to generate these local fracture orientations. We interpret the IFZ as the result of cutoff elongation strains generated by displacement gradients developed on the Ghost Dance fault (e.g.,

Fig. 3a). If fractures in the IFZ are indeed related to both tuff cooling and fault displacement, the Ghost Dance fault is at least as old as the Topopah Spring Tuff. Early activity on the Ghost Dance fault, or a west-dipping, normal fault very close to the position of the Ghost Dance fault, is also supported by a 1 km offset of the base Tertiary unconformity, interpreted from a seismic line across Yucca Mountain that was acquired in 1994 [Brocher et al., 1998].

The broader history of development of the Ghost Dance and Abandoned Wash faults is also illuminated by the displacement patterns illustrated in Fig. 7a,b. Displacement gradients along a fault result from the cumulative slip history and reflect fault growth and linkage [e.g., Childs et al., 1995; Ferrill et al., 1999a]. For example, displacement maxima and minima can be used to identify fault segments and provide insight into how small faults grow into larger faults [e.g., Ferrill et al., 1999a]. An individual fault segment is defined as a portion of a fault between two displacement minima and that exhibits a simple displacement maximum [Childs et al., 1995] (Fig. 7a,b). At the stratigraphic level being investigated, each fault segment would have propagated along strike from its initiation point, which now appears as the displacement maximum near the center of the segment [Childs et al., 1995]. Displacement patterns on the Ghost Dance and Abandoned Wash faults are consistent with the faults having propagated southward and northward respectively and established an overlap zone — an extensional fault relay ramp [e.g., Childs et al., 1995; Ferrill and Morris, 2001]. A connecting fault has been mapped [Day et al., 1995, 1998a] that breaches the ramp and connects the Ghost Dance and Abandoned Wash faults (Figs. 7 and 8). In common with many relay ramps, summing displacement on the Ghost Dance and Abandoned Wash faults reveals local decrease or deficit in the cumulative displacement in the area of overlap between the bounding faults [Childs et al.,

1995; Ferrill and Morris, 2001] (Fig. 7b). Such displacement deficits are compensated for by deformation processes other than slip on the principal bounding faults. Common modes of displacement compensation are increased synthetic bed dip in the relay ramp [e.g., Peacock and Sanderson, 1994; Huggins et al., 1995] or, as here, increased density of faulting and fracturing (Fig. 8). The area of overlap between the Ghost Dance and Abandoned Wash faults is one of general displacement deficit (Fig. 7b) and contains numerous small faults (Fig. 7a). Fault density (trace length per square km) is high in the general area of overlap ($5.2 \text{ km} / \text{km}^2$, see northern 1 km^2 in Fig. 8) and extremely high adjacent to the greatest displacement deficit ($10.1 \text{ km}/\text{km}^2$, see southern 1 km^2 in Fig. 8). The West Ridge connecting fault system is another example at Yucca Mountain where local fault density is associated with displacement gradients on larger scale faults (see analysis in Ferrill and Morris, 2001). As in the case of the IFZ, faults in the West Ridge connecting fault system have NW-SE trends and are not consistent with the dominant fault pattern. Instead, they represent local variability in smaller-scale fault block deformation. This variability is, in part, controlled by displacement patterns on block bounding faults.

5. Conclusions

Detailed analyses of the data available for Yucca Mountain reveals that relationships exist between smaller faults and fractures and the larger faults. In particular, displacement gradients on the larger faults have a strong influence on the orientation and distribution of

smaller faults and fractures. Two aspects of displacement gradient-driven deformation are cutoff elongation and displacement deficit compensation.

Cutoff elongation and the resulting distribution and orientation of fractures within fault blocks are sensitive to stress system and resulting slip directions at the time of faulting and initial bed orientation. Analyses of strains generated by fault displacement gradients indicate that many parts of Yucca Mountain may have experienced both extensional and contractional strains greater than 2 or 3 %, sufficient to generate fractures. The variable extension direction at Yucca Mountain since the inception of faulting (about 13 Ma) suggests that cumulative strain patterns are likely complex and strains generated by fault displacement are more pervasive than a single stress state “snapshot” would suggest. We have previously identified an area of interaction at Yucca Mountain between the Northern Windy Wash and Fatigue Wash faults [area 1 in Ferrill and Morris, 2001] (Fig. 1). This area, the West Ridge connecting fault system, has experienced high cutoff elongation clearly manifest as a zone of steeply southwest dipping strata containing a high concentration of mapped normal faults [Day et al., 1998a,b]. Both the Northern Windy Wash and Fatigue Wash faults, in the area of the West Ridge connecting fault system, exhibit high cutoff elongations (Fig. 5, Appendix 2).

Displacement deficit compensation is illustrated by the example of the Ghost Dance—Abandoned Wash fault system. The area of overlap between these two faults exhibits a marked cumulative displacement deficit. In addition, this area contains a large number of small faults oriented sub-parallel to the larger faults and contributing to the overall extension. The fault density in this locality is anomalously high, approximately twice that of surrounding areas outside the influence of the displacement deficit zone.

We have shown that there is considerable variability in terms of orientation and intensity in the fault and fracture framework of Yucca Mountain. It should be recognized that different fault blocks experience different deformation histories, producing different strain states. Analysis of the fault and fracture framework of any fault block would benefit from considering the possibility that displacement gradients on bounding faults have influenced strain intensity and hence caused variability in the orientation and intensity of small-scale faulting and fracturing.

Appendices

Appendix 1. Fault and fracture data from the Exploratory Studies Facility are available in electronic format from http://m-oext.ymp.gov/html/prod/db_tdp/sep/internet/default.htm. Data from the following files were used in this paper:

9606006A, 9606006B, 9609018, 9609020, 9708014A, 9708014B, 9711020, 9711021, 9711022, 9711023, 9711024, 9711025, 9711027.

Appendix 2. A series of 15 cutoff elongation maps were generated to illustrate the influence of stress tensor R value (see equation in Section 3.1.1), direction of extension (σ_3), and stratal orientation (dip) at the time of fault initiation. These cutoff elongation maps are illustrated in Fig. A1, and controlling parameters are provided in Table A1.

Table A1. Magnitudes of maximum (σ_1), intermediate (σ_2), and minimum (σ_3) principal compressive stresses, R values, extension directions, and original bed dips used for cutoff elongation analyses are shown in maps A through O in Appendix 2

Map in					Extension	Original
Appendix 2	σ_1	σ_2	σ_3	R	Direction	Bed Dip
A	21	19	6	0.13	270	0
B	21	17	6	0.27	270	0
C	21	15	6	0.40	270	0
D	21	13	6	0.53	270	0
E	21	11	6	0.67	270	0
F	21	17	6	0.27	260	0
G	21	17	6	0.27	270	0
H	21	17	6	0.27	280	0
I	21	17	6	0.27	290	0
J	21	17	6	0.27	300	0
K	21	17	6	0.27	270	0
L	21	17	6	0.27	270	2
M	21	17	6	0.27	270	4
N	21	17	6	0.27	270	6
O	21	17	6	0.27	270	8

Acknowledgments

This paper was prepared to document work performed by the Center for Nuclear Waste Regulatory Analyses (CNWRA) for the U.S. Nuclear Regulatory Commission (NRC) under contract No. NRC-02-97-009. The activities reported here were performed on behalf of the NRC Office of Nuclear Material Safety and Safeguards, Division of Waste Management. This paper is an independent product of the CNWRA and does not necessarily reflect the views or regulatory position of the NRC. We thank Philip Justus for many discussions regarding faults and fractures at Yucca Mountain. Reviews by H. Larry McKague, John Stamatakos and Wesley Patrick significantly improved earlier versions of this paper. We also thank Rebecca Emmot for her assistance with manuscript preparation.

References

- Atwater, T. Implications of plate tectonics for the Cenozoic tectonic evolution of western North America. *Geol. Soc. Am. Bull.*, 81. 3513–3536, 1970.
- Barton, C. C., and P. A. Hsieh, Physical and hydrologic-flow properties of fractures. Washington, DC: *Am. Geophys. Union*, 1989.
- Barton, C. C., and E. Larsen, Fractal Geometry of Two-Dimension Fracture Networks at Yucca Mountain. *Fundamentals of Rock Joints: Proc. of the International Symp. on Fundamentals of Rock Joints*. O. Stephanson, ed. Sweden, Bjorkliden, pp. 77–84, 1985.

- Barton, C. C., E. Larsen, W. R. Page, T. M. Howard, Characterizing Fractured Rock for Fluid-Flow, Geomechanical, and Paleostress Modeling: Methods and Preliminary Results from Yucca Mountain, Nevada. *U.S. Geol. Surv. Open-File Rpt. 93-269*, 1993.
- Bott, M. H. P., The mechanics of oblique slip faulting. *Geological Magazine*, 96, 109–117, 1959.
- Buesch, D. C., and R. W. Spengler, Character of the middle nonlithophysal zone of the Topopah Spring Tuff at Yucca Mountain. *Proc. of the 8th International Conf. on High Level Radioactive Waste Management*, 16–23, 1998.
- Brocher, T. M., W. C. Hunter, and V. E. Langenheim, Implications of Seismic Reflection and Potential Field Geophysical Data on the Structure Frame Work of Yucca Mountain—Crater Flat Region, Nevada. *Geol. Soc. Am. Bull.*, 110. 947–971, 1998.
- Carr, W. J., Styles of Extension in the Nevada Test Site Region, Southern Walker Lane Belt; An Integrated Volcano-Tectonic and Detachment Fault Model. *Geol. Soc. Am. Memoir 176*, 283–303, 1990.
- CRWMS M&O, Geologic Framework Model (GFM 3.1) Analysis model report. MDL-NBS-GS-000002 Rev 00 ICN 01. Las Vegas, Nevada: CRWMS M&O, ACC: MOL. 20000121.0115, 2000.
- CRWMS M&O, Yucca Mountain Science and Engineering Report. DOE/RW-0539. Las Vegas, Nevada: DOE, Office of Civilian Radioactive Waste Management, Yucca Mountain Site Characterization Office, 2001.
- Childs, C., J. Watterson, J. J. Walsh, Fault overlap zones within developing normal fault systems. *J. Geol. Soc., London* 152, 535–549, 1995.

- Connor, C. B., and B. E. Hill, Three nonhomogeneous Poisson models for the probability of basaltic volcanism: Application to the Yucca Mountain region, Nevada. *J. Geophys. Res.*, 94, 10,107–10,125, 1995.
- Connor, C. B., J. A. Stamatakos, D. A. Ferrill, B. E. Hill, G. I. Ofoegbu, F. M. Conway, B. Sagar, and J. Trapp, Geologic Factors Controlling Patterns of Small-Volume Basaltic Volcanism: Application to a Volcanic Hazard Assessment at Yucca Mountain, Nevada. *J. Geophys. Res.*, 105, 407–432, 2000.
- Dawers, N. H., and M. H. Anders, Displacement-Length Scaling and Fault Linkage. *J. Struct. Geol.*, 17, 607–614, 1995.
- Day, W. C., R. P. Dickerson, C. J. Potter, D. S. Sweetkind, C. A. San Juan, R. M. Drake, II, C. J. Fridrich, Bedrock geologic map of the Yucca Mountain area, Nye County, Nevada, *U.S. Geol. Surv. Misc. Invest. Ser. Map, I-2627*, 1998a.
- Day, W. C., C. J. Potter, D. S. Sweetkind, R. P. Dickerson, and C. A. San Juan. Bedrock Geologic Map of the Central Block Area, Yucca Mountain, Nye County, Nevada, *U.S. Geol. Surv. Misc. Invest. Ser. Map, I-2601*, 1998b.
- Ferrill, D. A., Morris, A. P., Displacement gradient and deformation in normal fault systems. *J. Struct. Geol.*, 23, 619–638, 2001.
- Ferrill, D. A., J. A. Stamatakos, and D. Sims. Normal Fault Corrugation: Implications for Growth and Seismicity of Active Normal Faults. *J. Struct. Geol.*, 21, 1,027–1,038, 1999a.
- Ferrill, D. A., J. Winterle, G. Wittmeyer, D. Sims, S. Colton, A. Armstrong, A. P. Morris, Stressed rock strains groundwater at Yucca Mountain, Nevada. *GSA Today*, 9(5), 1–8, 1999b.

- Ferrill, D. A., J. A. Stamatakos, S. M. Jones, B. Rahe, H. L. McKague, R. H. Martin, and A. P. Morris, Quaternary Slip History of the Bare Mountain Fault (Nevada) from the Morphology and Distribution of Alluvial Fan Deposits. *Geology*, 24, 559–562, 1996a.
- Ferrill, D. A., G. L. Stirewalt, D. B. Henderson, J. A. Stamatakos, K. H. Spivey, and B. P. Wernicke, Faulting in the Yucca Mountain Region, Critical Review and Analyses of Tectonic Data from the Central Basin and Range. NUREG/CR–6401. Washington, DC: NRC, 1996b.
- Fridrich, C. J., Tectonic Evolution of the Crater Flat Basin, Yucca Mountain Region, Nevada, in Cenozoic Basins of the Death Valley Region. L. Wright and B. Troxel, eds. *Geol. Soc. Am. Special Paper 333*, 169–196, 1999.
- Harmsen, S. C. The Little Skull Mountain, Nevada, Earthquake of 29 June 1992: Aftershock Focal Mechanisms and Tectonic Stress Field Implications. *Bull. Seismol. Soc. Am.*, 84, 1,484–1,505, 1994.
- Hoek, E. and E.T. Brown, The Hoek-Brown Failure Criterion—A 1988 Update. *15th Canadian Rock Mechanics Symp.*, 31–38, 1988.
- Huggins, P., J. Watterson, J. J. Walsh, and C. Childs. Relay Zone Geometry and Displacement Transfer Between Normal Faults Recorded in Coal-Mine Plans. *J. Struct. Geol.*, 17, 1,741–1,755, 1995.
- Mandl, G., Mechanics of Tectonic Faulting, *Elsevier*, New York, 1988.
- Mongano, G. S., W. L. Singleton, T. C. Moyer, S. C. Beason, G. L. W. Eatman, A. L. Albin, and R. C. Lung, Geology of the Enhanced Characterization of the Repository Block Cross

- Drift – Exploratory Studies Facility, Yucca Mountain Project, Yucca Mountain, Nevada.
Denver, CO: Bureau of Reclamation and U.S. Geol. Surv., 1999.
- Morris, A. P., D. A. Ferrill, and D. B. Henderson, Slip tendency analysis and fault reactivation.
Geology, 24, 275–278, 1996.
- Oldow, J.S., Late Cenozoic Displacement Partitioning in the Northwestern Great Basin.
Geological Society of Nevada, Proceedings Volume, Walker Lane Symposium,
Structure, Tectonics & Mineralization of the Walker Lane, 17–52, 1992.
- Peacock, D. C. P., and D. J. Sanderson, Geometry and Development of Relay Ramps in Normal
Fault Systems. *Am. Assoc. Petrol. Geol. Bull.*, 78, 147–165, 1994.
- Sawyer, D. R., R. J. Fleck, M. A. Lanphere, R. G. Warren, D. E. Broxton, and M. R. Hudson.
Episodic Caldera Volcanism in the Miocene Southwestern Nevada Volcanic Field:
Revised Stratigraphic Framework, $^{40}\text{Ar}/^{39}\text{Ar}$ Geochronology, and Implications for
Magmatism and Extension. *Geol. Soc. Am. Bull.*, 106, 1,304–1,318, 1994.
- Scott, R. B. and J. Bonk. Preliminary Geologic Map of Yucca Mountain, Nye County, Nevada
with Geologics. U.S. Geological Survey Open-File Report 84-494, *U.S. Geol. Surv.*,
1984.
- Simonds, W. F., J. W. Whitney, K. Fox, A. Ramelli, J. C. Yount, M. D. Carr, C. D. Menges, R.
Dickerson, and R. B. Scott. Map of Fault Activity of the Yucca Mountain Area, Nye
County, Nevada. *U.S. Geol. Surv. Misc. Invest. Ser. Map*, I-2520, 1995.
- Snow, J. K. and B. P. Wernicke. Cenozoic Tectonism in the Central Basin and Range:
Magnitude, Rate, and Distribution of Upper Crustal Strain. *Am. J. Sci.*, 300, 659–719,
2000.

- Stock, J. M. and J. H. Healy. Stress Field at Yucca Mountain, Nevada, Geologic and Hydrologic Investigations of a Potential Nuclear Waste Disposal Site at Yucca Mountain, Southern Nevada. *U.S. Geol. Surv. Bull.* M. D. Carr and J. C. Yount, eds. 1790, 87–94, 1988.
- Sweetkind, D. S., L. O. Anna, S. C. Williams-Stroud, and J. A. Coe, Characterizing the Fracture Network at Yucca Mountain, Nevada, Part 1: Integration of Field Data for Numerical Simulations, Fractured Reservoirs. Characterization and Modeling Guidebook–1997. T. E. Hoak, P. K. Blomquist, and A. Klawitter, eds. Denver, Colorado: Rocky Mountain Assoc. Geol., 185–196, 1997.
- Trudgill, B., and J. Cartwright, Relay-Ramp Forms and Normal-Fault Linkages, Canyonlands National Park, Utah. *Geol. Soc. Amer. Bull.*, 106, 1,143–1,157, 1994.
- Twiss, R. J., and E. M. Moores. *Structural Geology*. New York, New York: W.H. Freeman and Company, 1992.
- U.S. Department of Energy, Viability Assessment of a Repository at Yucca Mountain, Volume 3: Total System Performance Assessment, DOE/RW-0508/V3. U.S. Dept. Energy, Office of Civilian Radioactive Waste Management, Yucca Mountain Site Characterization Office, Las Vegas, NV, 1998.
- U.S. Geological Survey, North America Shaded Relief Map, Editorial. U.S. Geol. Surv., EROS Data Center, Reston, Virginia. <<http://nationalatlas.gov/atlasftp.html>>, 1999.
- Young, S. R., A. P. Morris, and G. L. Stirewalt, Preliminary Structural Interpretation of Reflection Seismic Line AV–1. CNWRA 92–024. San Antonio, Texas: CNWRA, 1992a.
- Young, S. R., G. L. Stirewalt, and A. P. Morris, Geometric Models of Faulting at Yucca Mountain. CNWRA 92-008. San Antonio, Texas: CNWRA, 1992b.

Zoback, M. L., R. E. Anderson, and G. A. Thompson, Cainozoic Evolution of the State of Stress and Style of Tectonism of the Basin and Range Province of the Western United States. *Philosophical Transactions of the Royal Society of London, Royal Soc. of London, A300*, 407–434, 1981.

Figure captions

Figure 1. (a) Shaded relief map (from U.S. Geological Survey, 1999) showing location of Yucca Mountain within Walker Lane and Basin and Range physiographic province (after Twiss and Moores; Fig. 1 in Oldow, 1992). (b) Location map of Yucca Mountain illustrating principal faults (red lines) [Day et al., 1998a], and the surface projections of the two tunnels (blue lines): Exploratory Studies Facility (ESF), and the Enhanced Characterization of the Repository block (ECRB). Background is a Landsat Thematic Mapper image.

Figure 2. Views of the Geologic Framework Model version 3.1 [CRWMS M&O, 2000].

(a) View of the model from the ground surface down to the top of the Repository Host Horizon (RHH). (b) View of the model showing the top of the RHH and underlying stratigraphy to illustrate the fault gaps. The ESF is displayed as a solid yellow line where it lies above the RHH and a dashed yellow line where it lies within it. The Ghost Dance—Abandoned Wash fault system is highlighted by a gray rectangle. (c) View of the RHH cutoff lines against faults modeled within the Geologic Framework Model. The cutoff lines are used to construct fault surfaces between the hanging wall and footwall cutoff lines, the model is then placed in a stress tensor field - in this case σ_1 = vertical, 21 MPa, σ_2 = horizontal, azimuth 000°, 17 MPa, and σ_3 = horizontal, azimuth 270°, 6 MPa. Here bedding is assumed to have been horizontal prior to fault motion. Cutoff elongations are calculated for each segment of each cutoff line and displayed color-coded according to the scale.

Figure 3. Displacement gradients and distributed deformation. (a) Cutoff elongation strain developed as a result of a propagating normal fault. Deformation is depicted as being preferentially partitioned into the hanging wall because this is likely common at Yucca Mountain [Ferrill and Morris, 2001]. (b) Displacement deficit compensation and cutoff elongation within an extensional relay ramp combine to develop a network of small faults sub-parallel to, and a connecting fault oblique to the regional trend respectively.

Figure 4. Circular histograms of features indicating fault strikes at Yucca Mountain.

(a) Cumulative fault trace length {data from Geologic Framework Model version 3.1 [CRWMS M&O, 2000]}, (b) Fault segment length weighted by cumulative EW heave {data from Geologic Framework Model version 3.1 [CRWMS M&O, 2000]}, (c) Scarps and lineaments in alluvium indicating probable late Quaternary fault motion (data from Simonds et al., 1995), (d) Fault traces, bedrock-alluvium contacts and other features indicating possible late Quaternary fault motion (data from Simonds et al., 1995).

Figure 5a,b. Maps of traces of faults at Yucca Mountain where they intersect with the RHH {data extracted from the DOE Geologic Framework Model version 3.1 [CRWMS M&O, 2000]}. The cutoff elongation for each segment of the cutoff lines is displayed color-coded according to the scale in 2 % increments. All cutoff lines in each map are modeled as subject to the same stress tensor throughout the map and assuming the same initial (pre-faulting) bedding orientation, different maps illustrate different conditions of stress and initial bedding orientation and these conditions are shown in the inset at top right of each map. (a) Likely stress conditions

at Yucca Mountain 12.8 million years ago. (b) Likely stress conditions at Yucca Mountain now. Also shown are the locations of evidence for late Quaternary age faulting [Simonds et al., 1995]. (c) Detail of the West Ridge connecting fault system under conditions existing at 12.8 Ma. The high positive extensions on the sections of the Northern Windy Wash and Fatigue Wash faults correspond to the location of the connecting fault system that has developed to accommodate these strains. The actual geometry of the connecting fault system is more complicated than modeled by the DOE Geologic Framework Model [Day et al., 1998a; Ferrill and Morris, 2001].

Figure 6. East-west component of horizontal displacement (heave) on the major faults at Yucca Mountain. Plotted here are the heave profiles for the Solitario Canyon, Paintbrush Canyon, Northern Windy Wash, and Fatigue Wash faults. In addition, the cumulative (combined) heave of these four faults is shown together with the cumulative heave of all faults within the DOE Geologic Framework Model. Bold vertical lines at the ends of lines indicate the points at which the faults are truncated by the edges of the model.

Figure 7. The Ghost Dance—Abandoned Wash fault system. (a) Map from Day et al. [1998a] with the Ghost Dance and Abandoned Wash faults highlighted together with the connecting fault that breaches the extensional relay ramp between the two faults (see Fig. 8 for key). (b) Throw profiles of the Ghost Dance—Abandoned Wash fault system using data from the DOE Geologic Framework Model [CRWMS M&O, 2000]. (c) Outline map illustrating segment analysis of the Ghost Dance—Abandoned Wash fault system. Also shown are the predominant fault and

fracture orientations for each 500 m section of the ESF Main Drift, and the fracture frequency ($f/5$ m) profile (calculated at 5 meter intervals) along the Main Drift of the ESF [Mongano et al., 1999].

Figure 8. Detail from geological map by Day et al. [1998a]. The two, one-kilometer-square areas used to calculate the fault densities are outlined. Fault density for the southern area, which contains the fault network developed as a result of displacement deficit in the linked Ghost Dance—Abandoned Wash fault system, is approximately 10.1 km/km^2 . Fault density in the northern area is approximately 5.2 km/km^2 .

Figure A1. Cutoff elongation maps of Yucca Mountain faults based on data extracted from the DOE Geologic Framework Model [CRWMS M&O, 2000], cutoff lines are color-coded according to the scale from -10 % to +10 % in 2 % increments. Values and orientations of the principal stresses and initial stratal orientations for each map are given in Table A1.

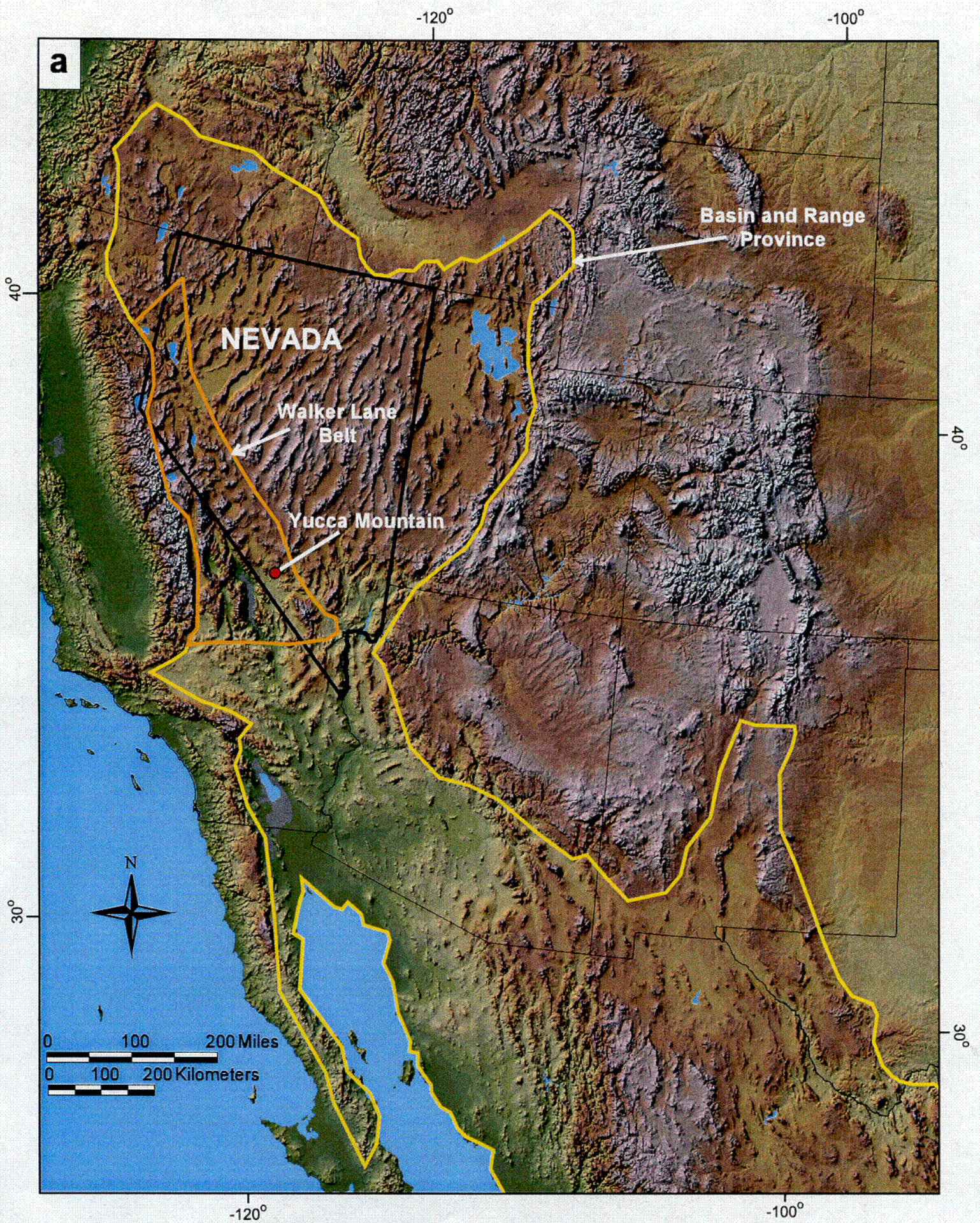


Figure 1a
Morris et al.

COI

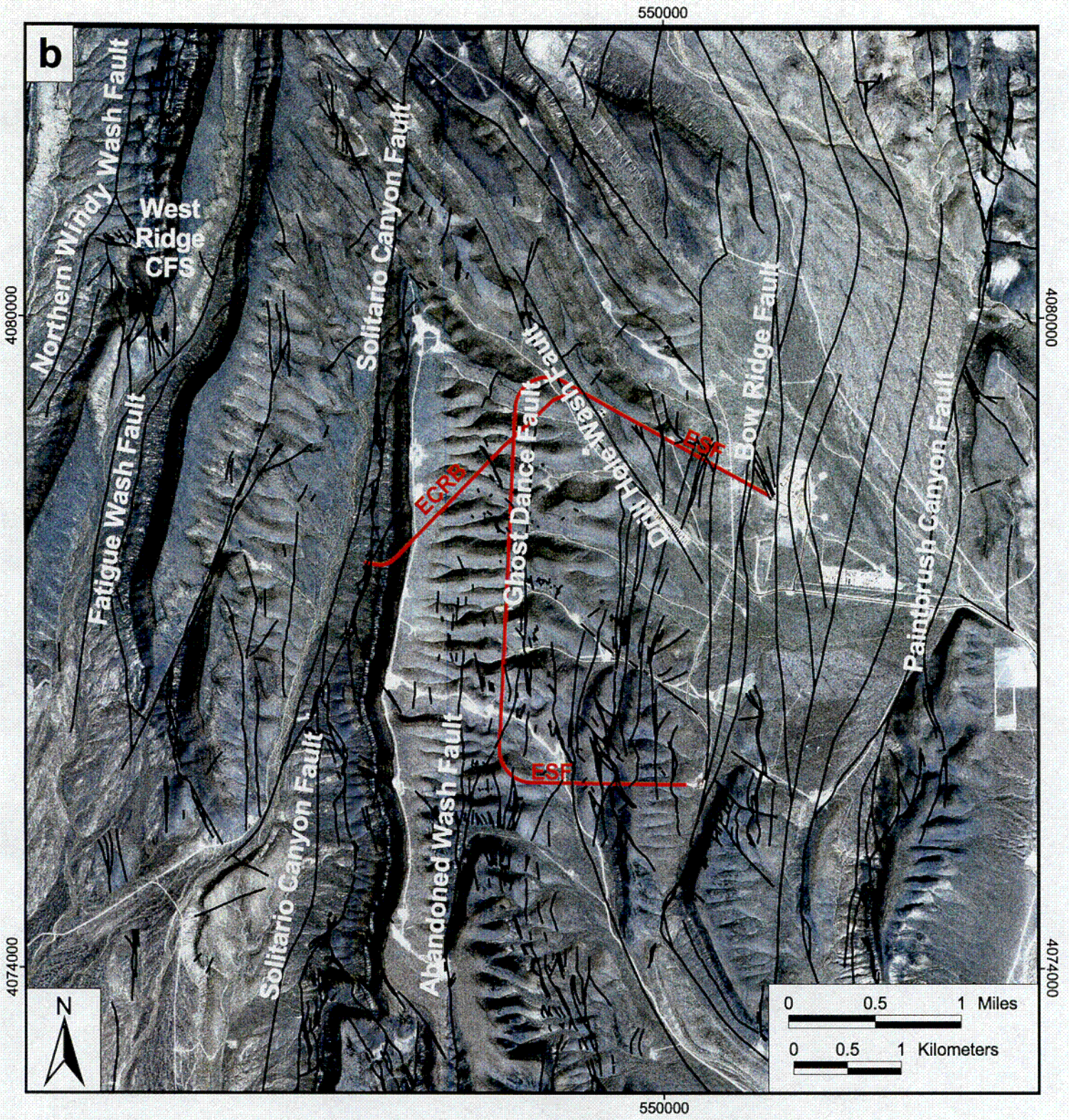
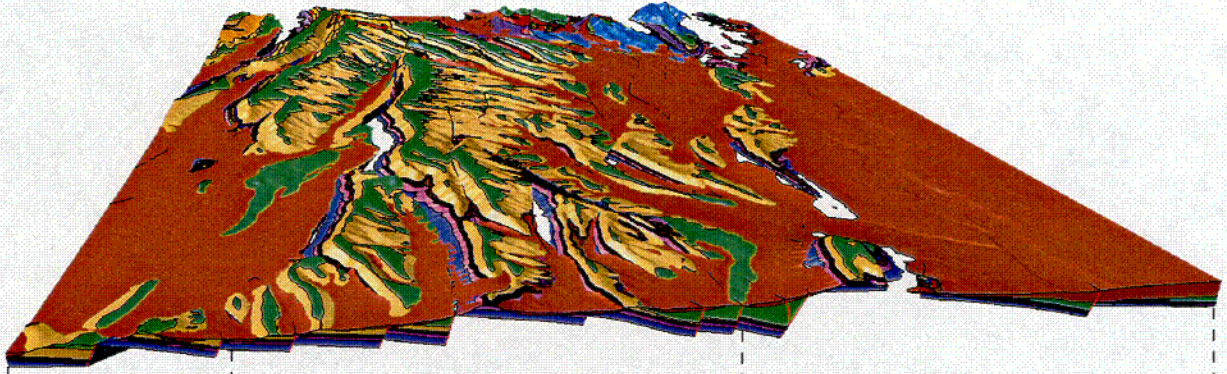


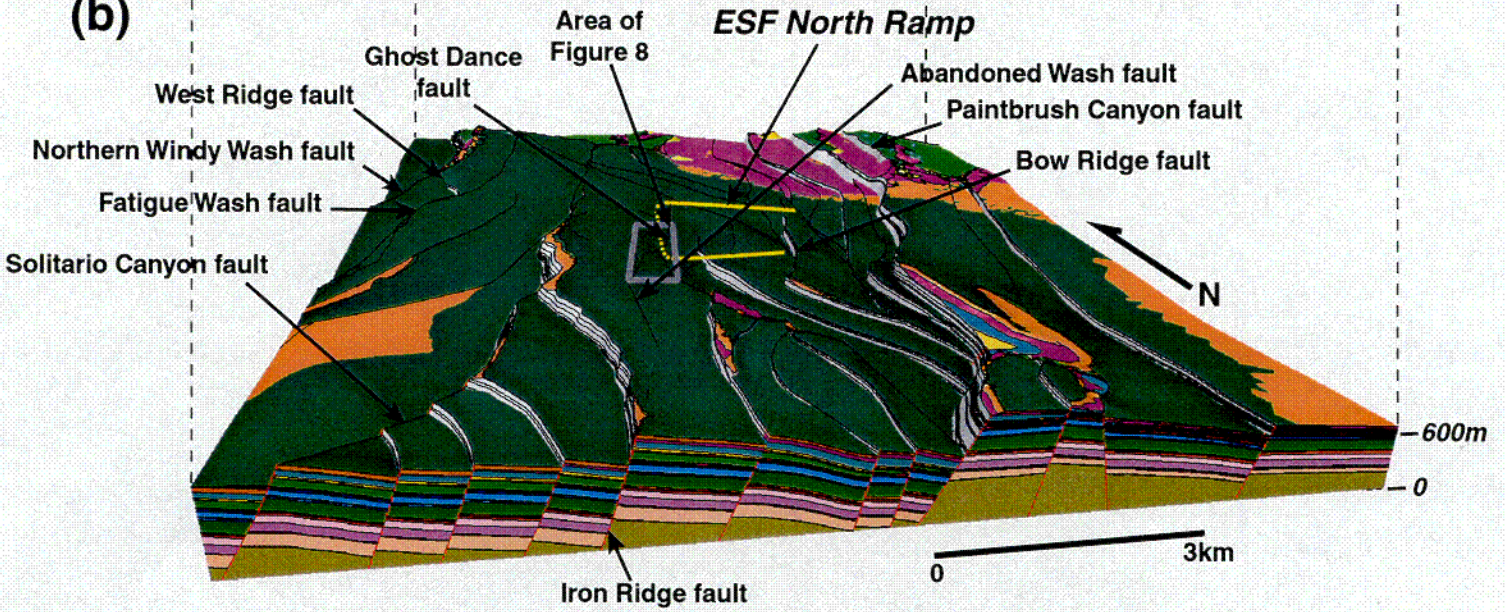
Figure 1b
Morris et al.

C02

(a)



(b)



(c)

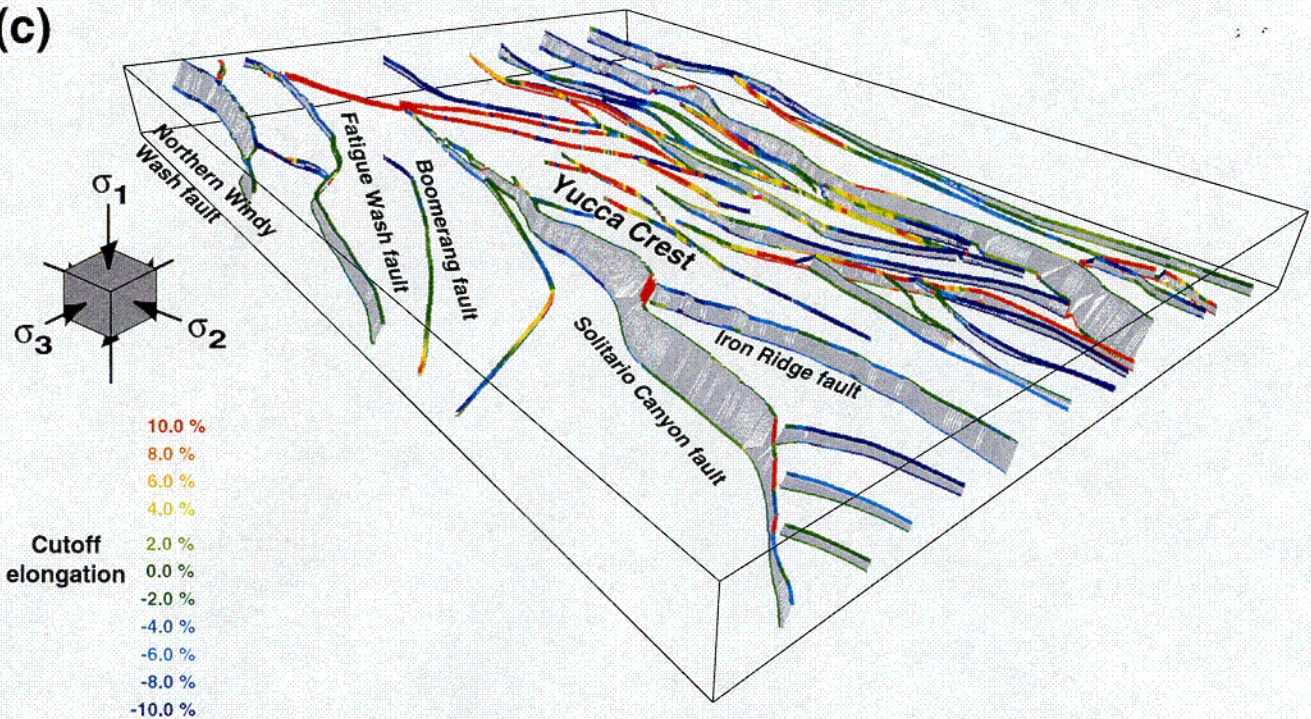
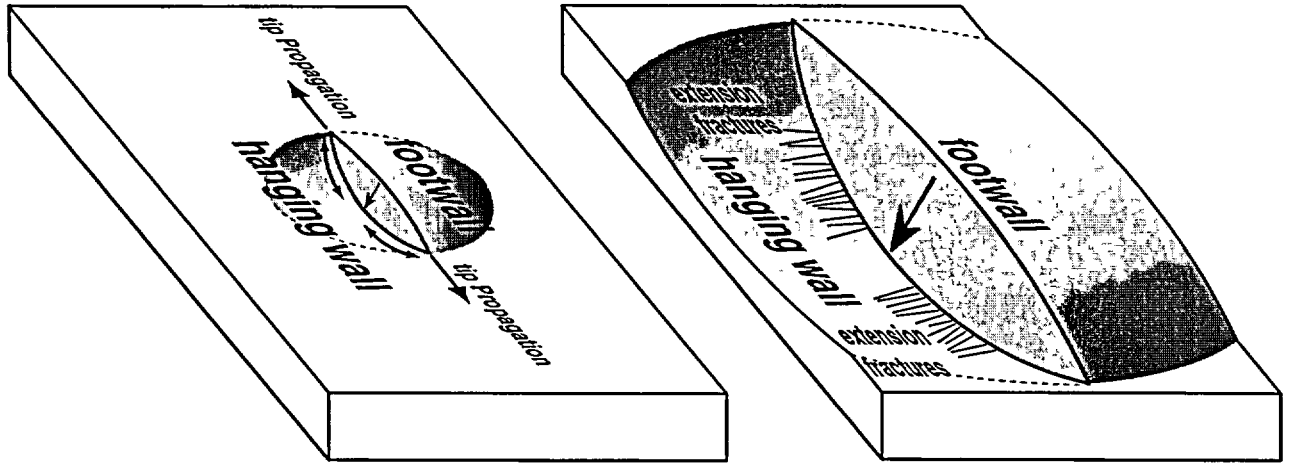


Figure 2
Morris et al.

003

(a)



(b)

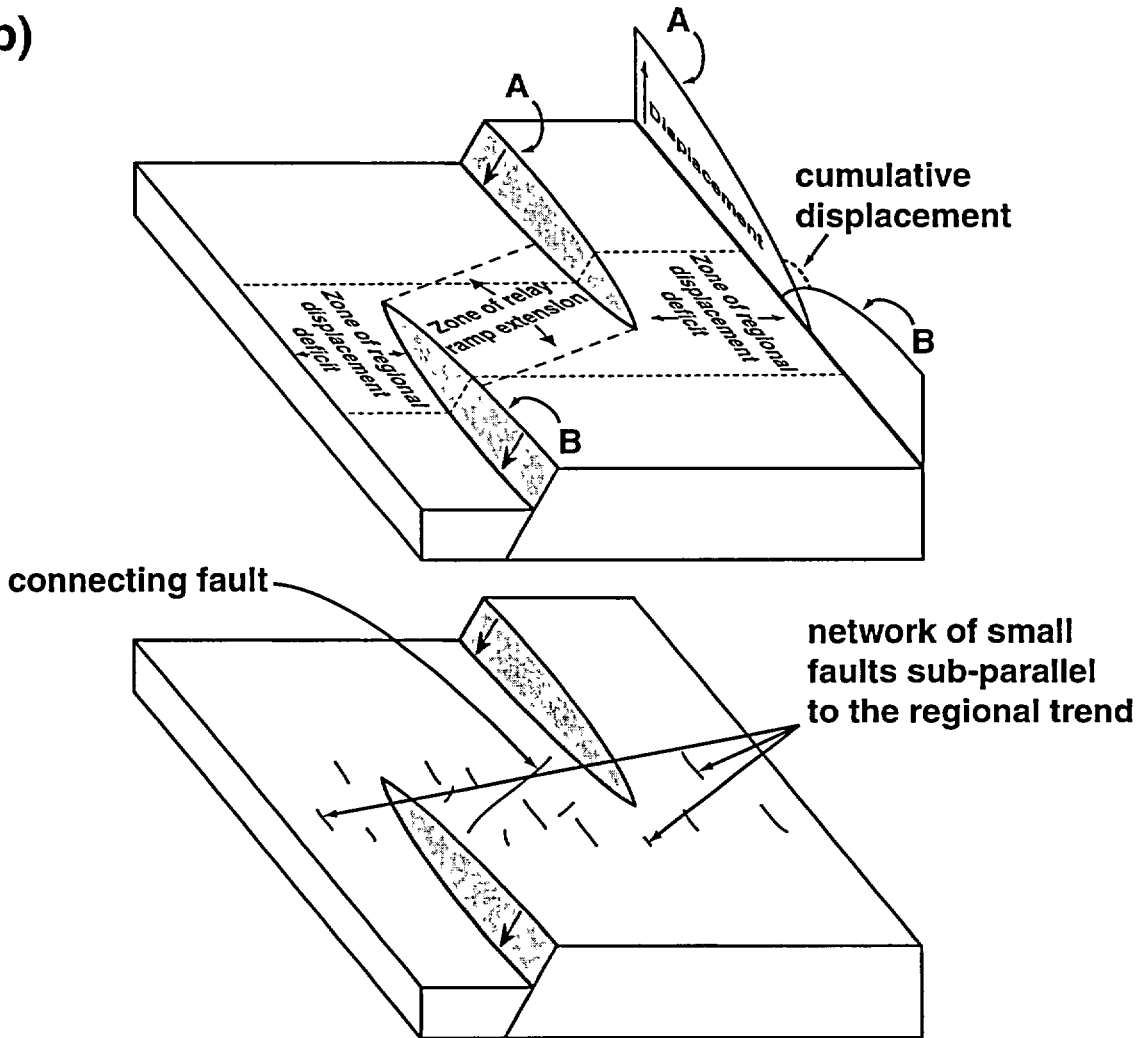
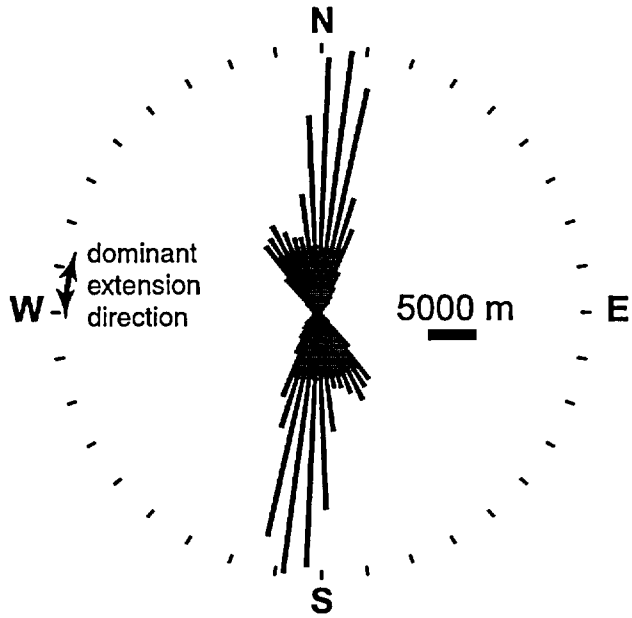
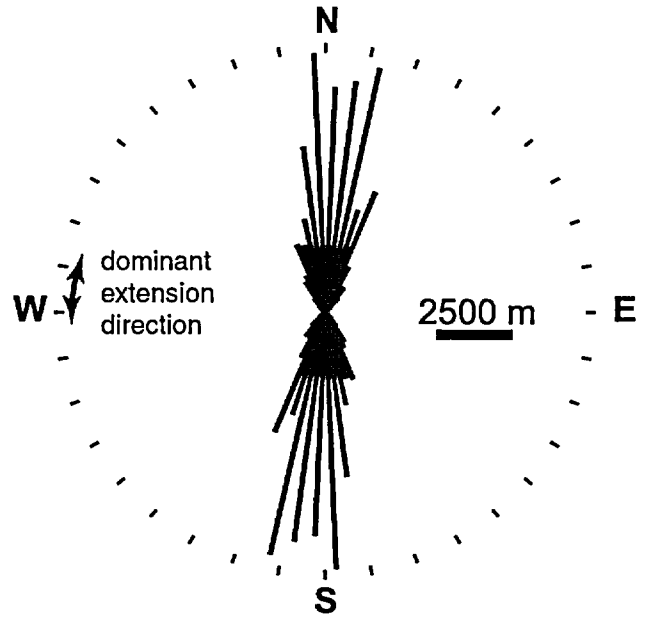


Figure 3
Morris et al.

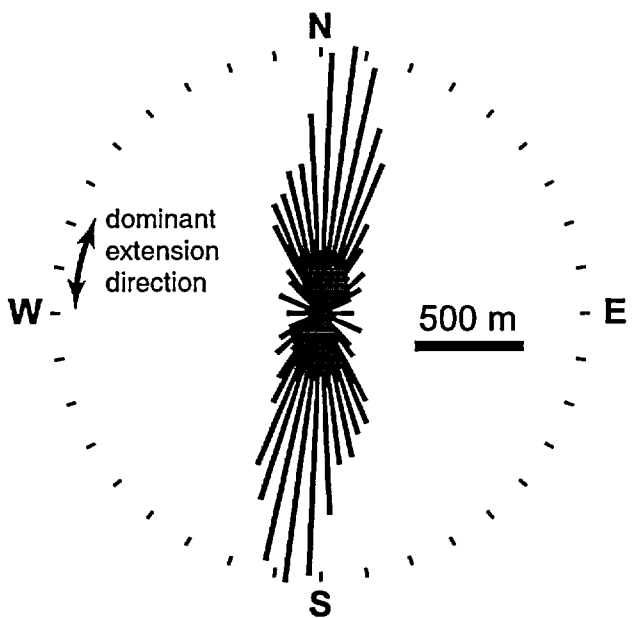
(a)



(b)



(c)



(d)

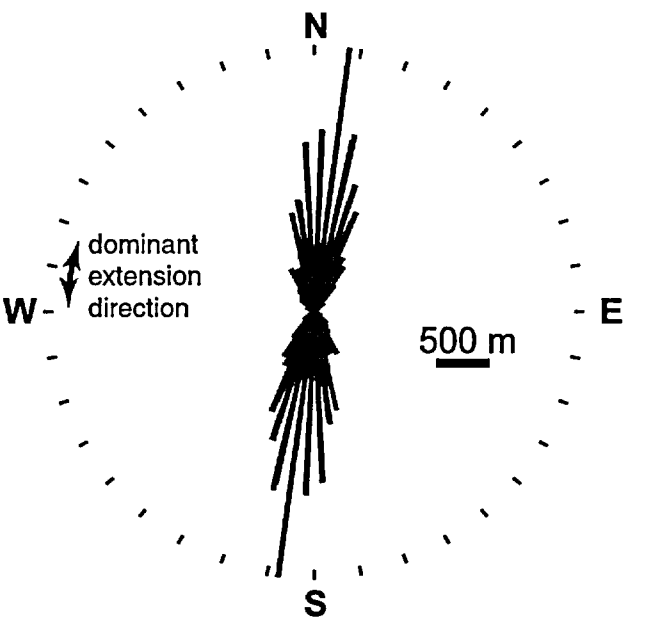
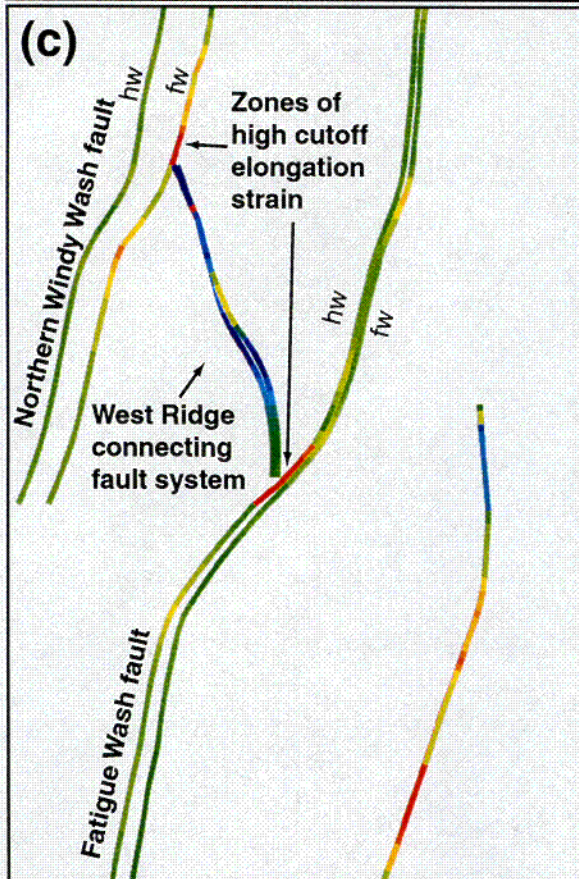
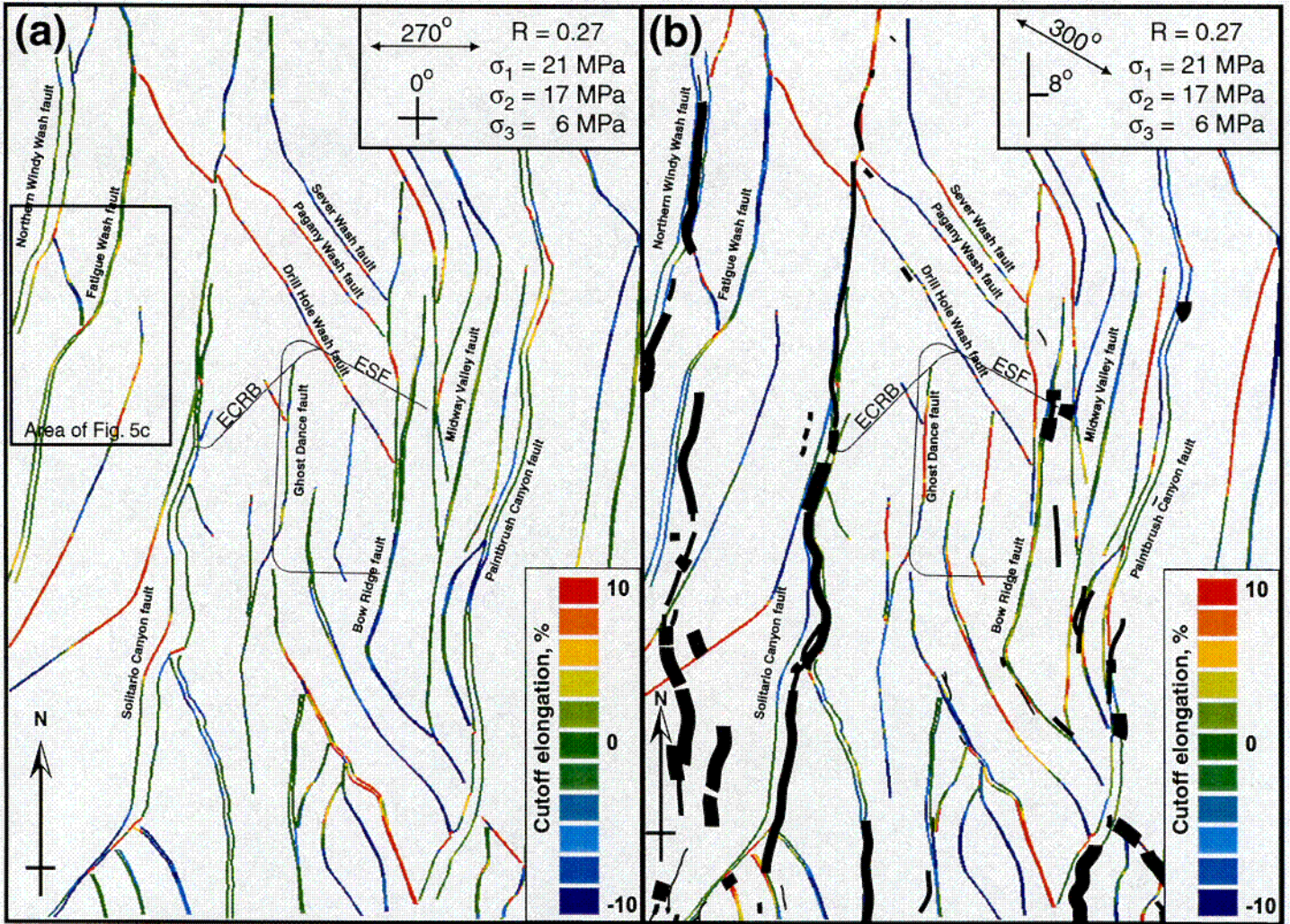


Figure 4
Morris et al.



-  **Known late Quaternary fault movement**
Scarp in alluvial materials, traceable fault or fracture
-  **Suspected late Quaternary fault movement**
Scarp at bedrock-alluvium contact
-  **Suspected late Quaternary fault movement**
Traceable fault, suspected fault contact, lineament
-  **Unknown age of faulting**
Scarp in bedrock

Figure 5
 Morris et al.

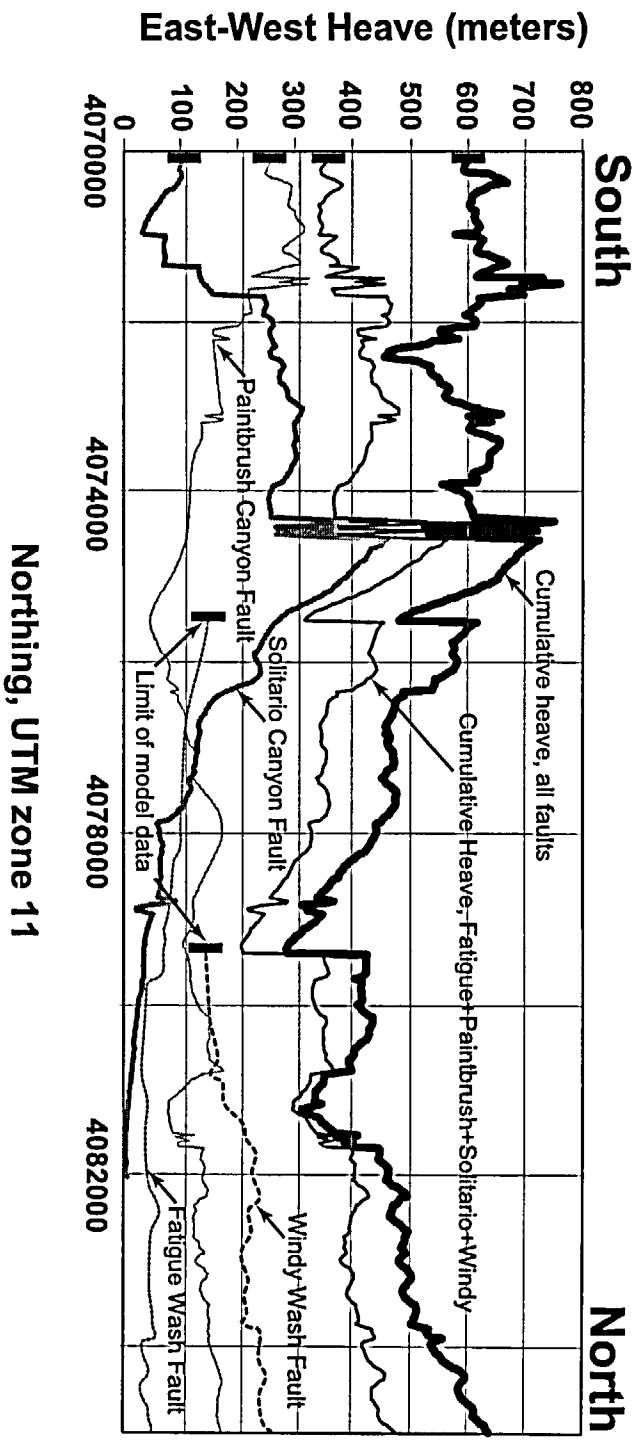
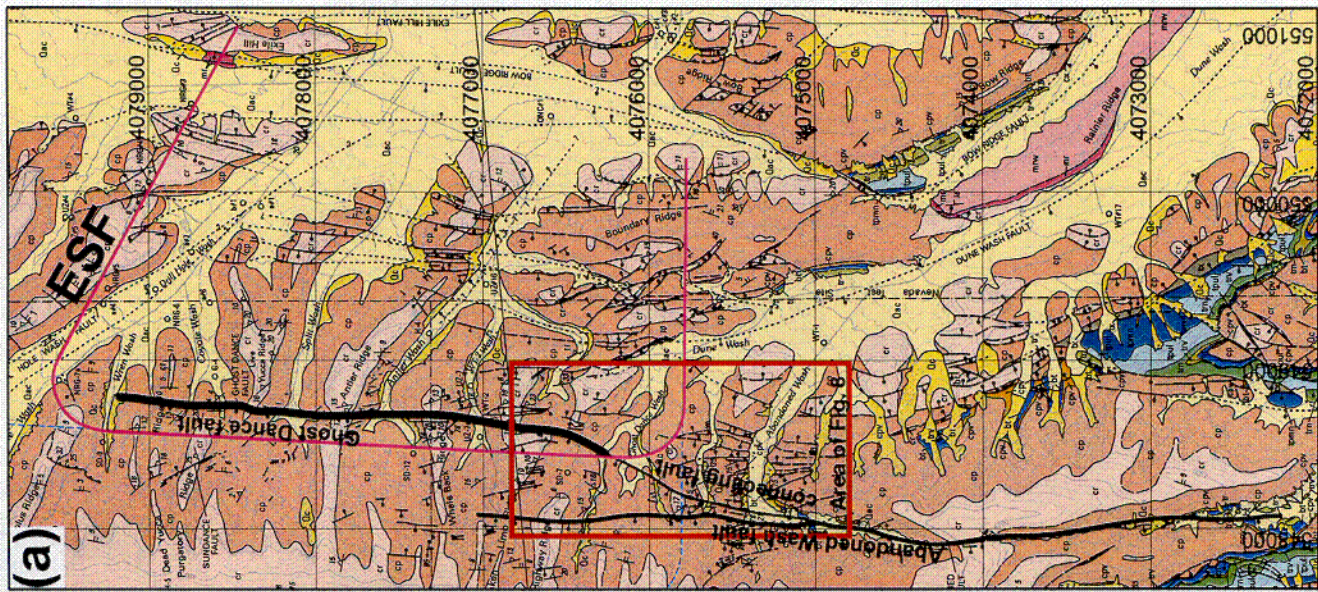
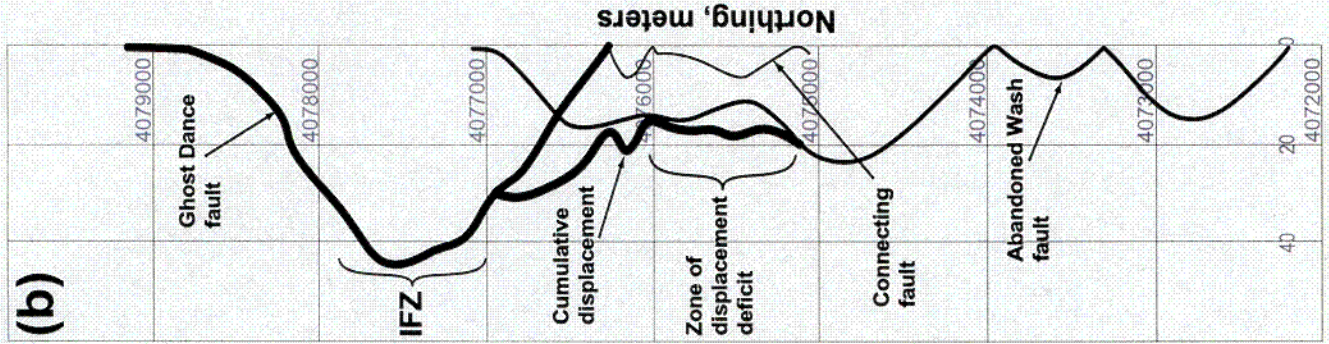


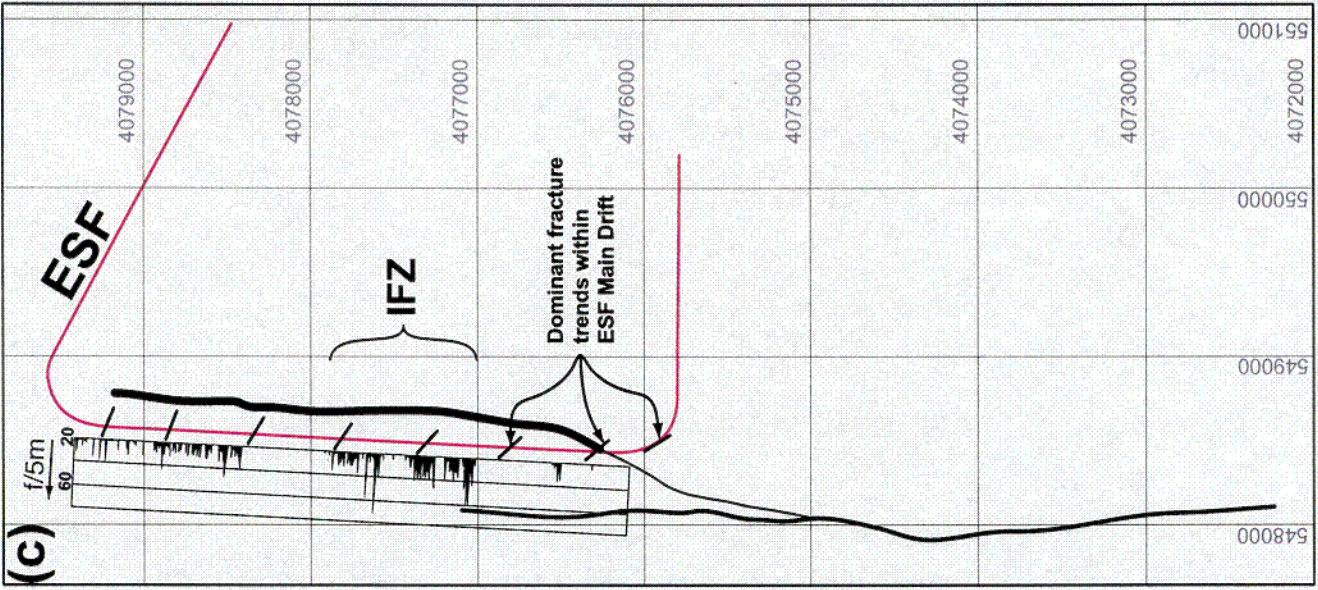
Figure 6
Morris et al.



Easting, meters



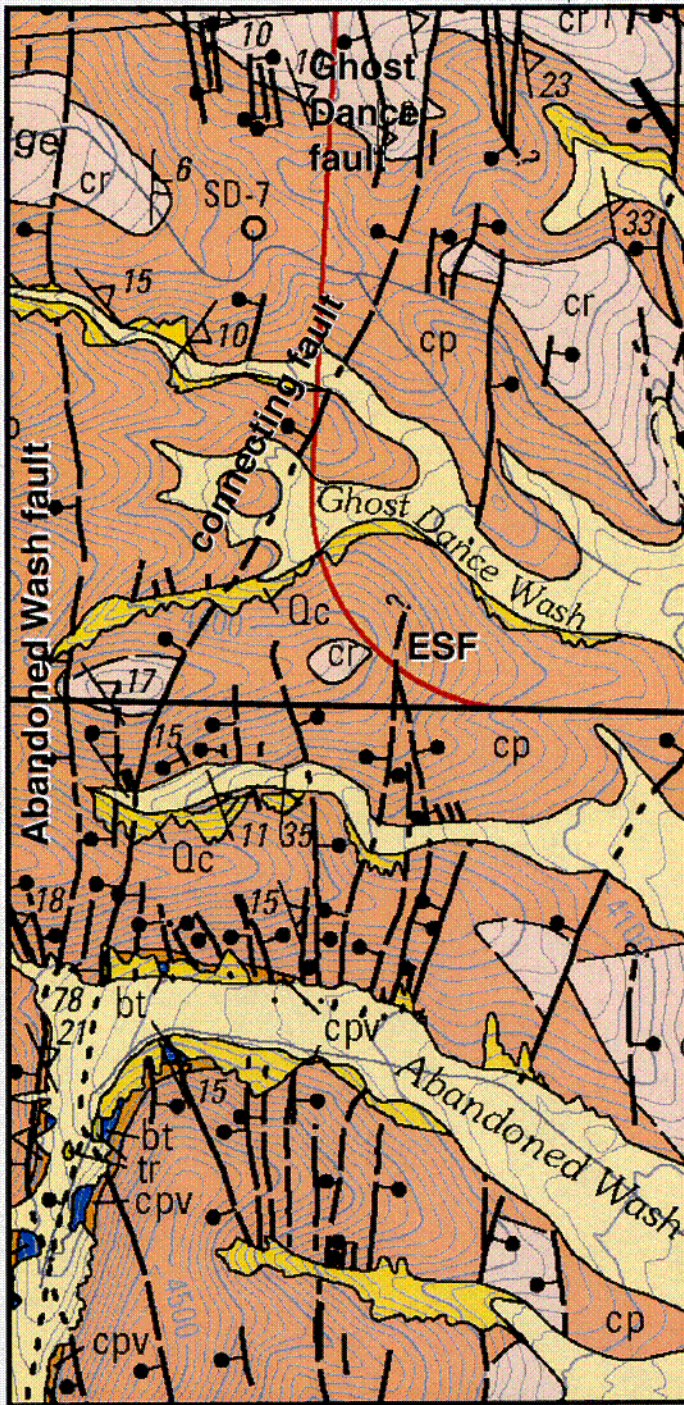
Throw, meters



Easting, meters

Figure 7
Morris et al.

Fault density = 5.2 km/km²



Fault density = 10.1 km/km²

Map Legend

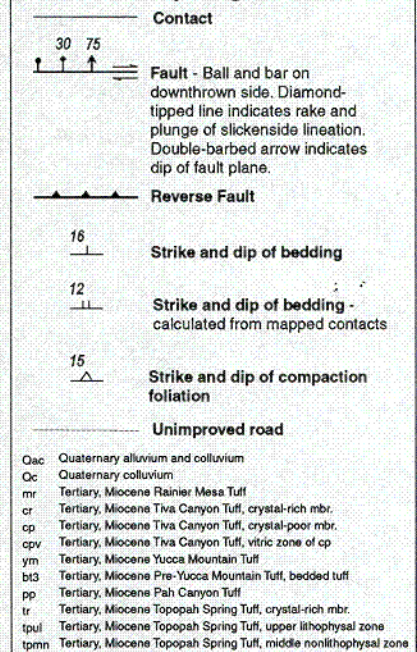


Figure 8
Morris et al.

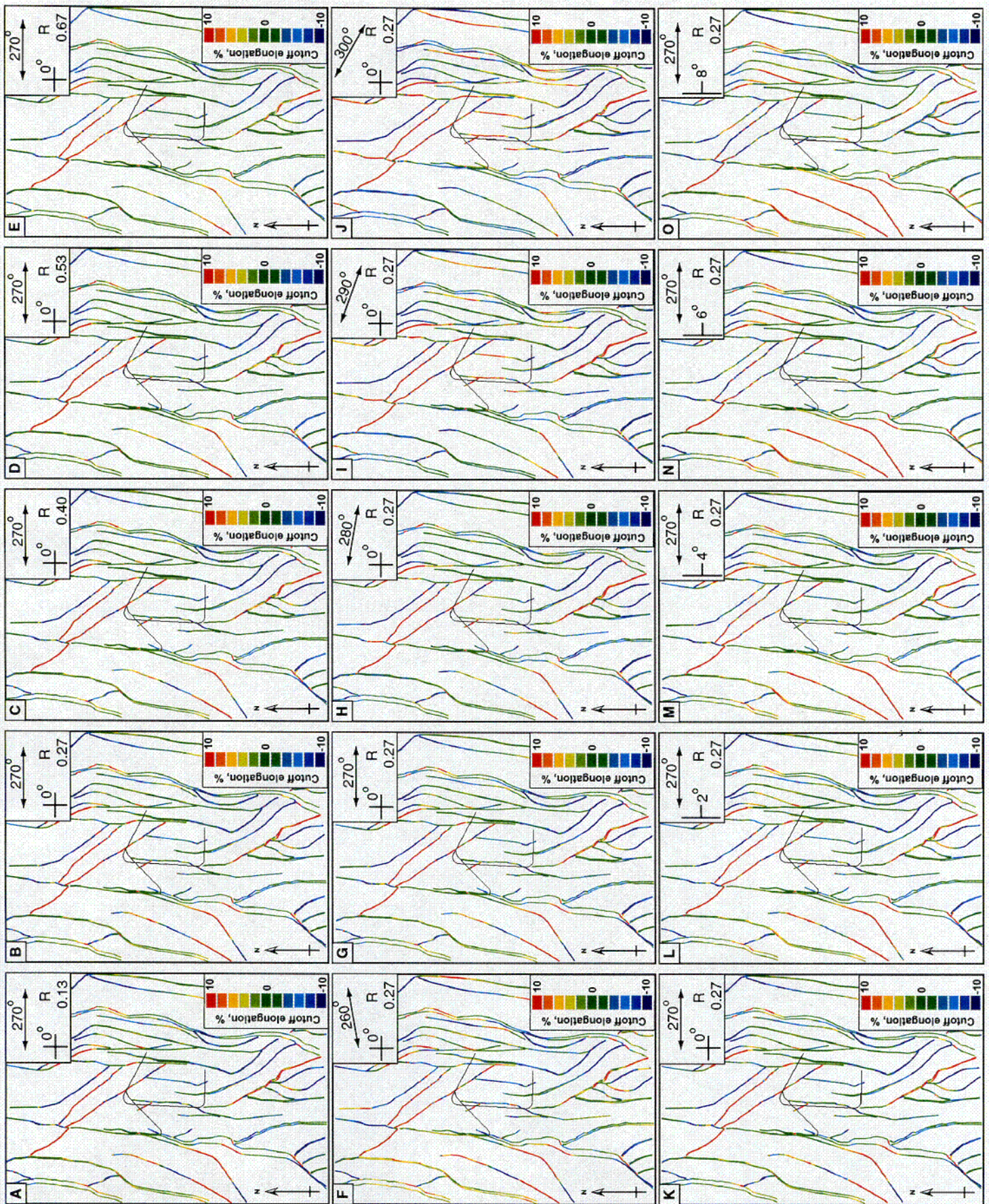


Figure A1
Morris et al.